Enhanced Real-Time Ultrasound Elastography with Phase Gradient

Enrique González-Mateo, Francisco Camarena, Noé Jiménez
Email: engonma@upv.edu
Instituto de Instrumentación para Imagen Molecular, Universitat Politècnica de València - CSIC, Camino de Vera s/n, 46022, València, Spain

***Abstract*—Elastography is a well-practiced, non-invasive technique for imaging mechanical deformations to quantify the stiffness of tissues. The current methods of estimating shear wave velocity may often be troubled by issues of viscoelastic dispersion and computational complexity. A new algorithm is proposed in this paper, where a combination of the angular spectrum method and a local phase gradient estimator improves wavenumber determination in shear wave elastography. Testing on phantoms with homogeneous, rigid, and soft inclusions was performed by this algorithm. The average phase velocity obtained in the phase velocity map was 1.58 m/s with a standard deviation of 0.05 m/s for the homogeneous phantom. On the other hand, in heterogeneous phantoms, velocities ranged from 1 to 3 m/s. The method achieved an average reconstruction time of 0.253 s by averaging over nine frequency bands and two push locations. This algorithm achieves much-reduced computational complexity for high accuracy scanning; therefore, it offers a great improvement toward real-time elastography applications.**

***Index Terms*—Shear-wave elastography, Phase-gradient, Directional filter**

I. Introduction

Elastography is an imaging technique that employs the application of mechanical forces and subsequent analysis of tissue deformation to quantify tissue stiffness. Tissues with lower stiffness deform to a greater extent when subjected to stress, whereas those with higher stiffness deform to a lesser extent. Techniques such as ultrasound [2] and MRI [1] are employed to track these deformations, with the resulting data used to calculate the tissue's elastic modulus, or stiffness. In more sophisticated methodologies, such as shear wave elastography (SWE) [3], the velocity of shear waves traversing through biological tissues is quantified to generate intricate stiffness maps. The images, known as elastograms, offer valuable insights for the diagnosis of conditions such as cancer [5], liver assesment [4] or thyroid nodule evaluation [6] by highlighting differences in tissue mechanical properties.

At present, the accurate and robust acquisition of elasticity maps represents a significant challenge in the field of transverse wave elastography. A review of the literature reveals a multitude of time-domain-based techniques for calculating wave velocity through time-of-flight (TOF) measurements [8]. However, these methods fail to account for the dispersion of materials due to viscoelasticity and geometry [7]. Consequently, techniques based on the frequency domain, such as gradient-phase [9] or Fourier transform methods [10], have emerged as a solution. However, the computational costs associated with calculating the wavenumber of the propagating waves using spatiotemporal Fourier transforms [11] and iterative processing [12] are considerable.

This work reports the findings from the Algorithms for Mapping Elastic Modulus (a-MEM) Challenge 2024, held at the IUS 2024 conference, organized by the IEEE UFFC-JS. The challenge underscores the critical need for robust methodologies in elasticity mapping. In response, we propose a novel algorithm for wavenumber determination that integrates the angular spectrum method with a local phase gradient estimator. This approach is characterized by its low complexity, facilitating its application in real-time scenarios.

II. Methods

The phase gradient-based method is employed to determine the phase velocity of shear waves at various frequencies. A detailed explanation of the methodology is provided in the subsequent section, with a summary presented in Fig. 1. To estimate tissue motion, denoted as $u(x, z, t)$, the initial data must include in-phase and quadrature (IQ) images reconstructed after tissue excitation. These images enable the evaluation of the tissue velocity field using a two-dimensional autocorrelation method [13]. The velocity is calculated by comparing a reference signal with a time-shifted signal, and the phase shift is measured relative to a known frequency.

The temporal data are then transformed into the frequency domain $U(x, z, \omega)$ using a one-dimensional Fourier transform (F_{1D}). The frequency data are analyzed, and a frame $U(x, z, \omega_0)$ corresponding to the study frequency ω_0, where wave propagation is prominent, is selected. To improve accuracy in phase velocity estimation, noise is reduced using various filters. The data are further transformed into k-space $U(k_x, k_z, \omega_0)$ through a two-dimensional Fourier transform (F_{2D}) along the spatial dimensions. A wavenumber bandpass filter [15] is applied to eliminate spatial wavelengths outside the 0.5–11 m/s range. The method assumes the presence of a plane shear wave, and directional filtering is used to isolate shear waves propagating in the desired direction [16], facilitating the decomposition of tissue motion into plane

This research has been supported by the Ministerio Español de Ciencia e Innovación grant RYC2021-034920-I, and by Agencia Estatal de Investigación grants PID2022-142719OB-C21 and CNS2023-145707 funded by MCIN/AEI/10.13039/501100011033; Agència Valenciana de la Innovació grants INNVA2/2022/11 and INNEST/2022/345.

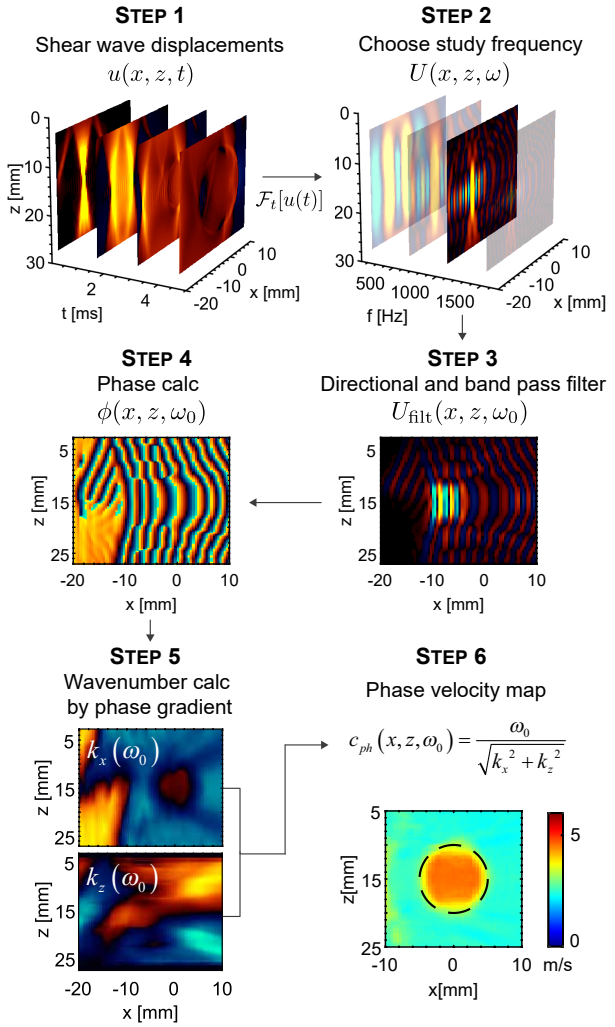


Fig. 1. Steps Graphical scheme of the local phase gradient method. This method takes the shear waves displacements as input (1). These displacements are then analyzed at a specific frequency (2) and directional and bandpass filtered (3). Once the dataset is clean, the phase is calculated (4) with the objective of knowing the wavenumber maps by a phase-gradient approach (5). Calculating the wavenumber in both the axial and lateral directions allows us to reconstruct the phase velocity map (6).

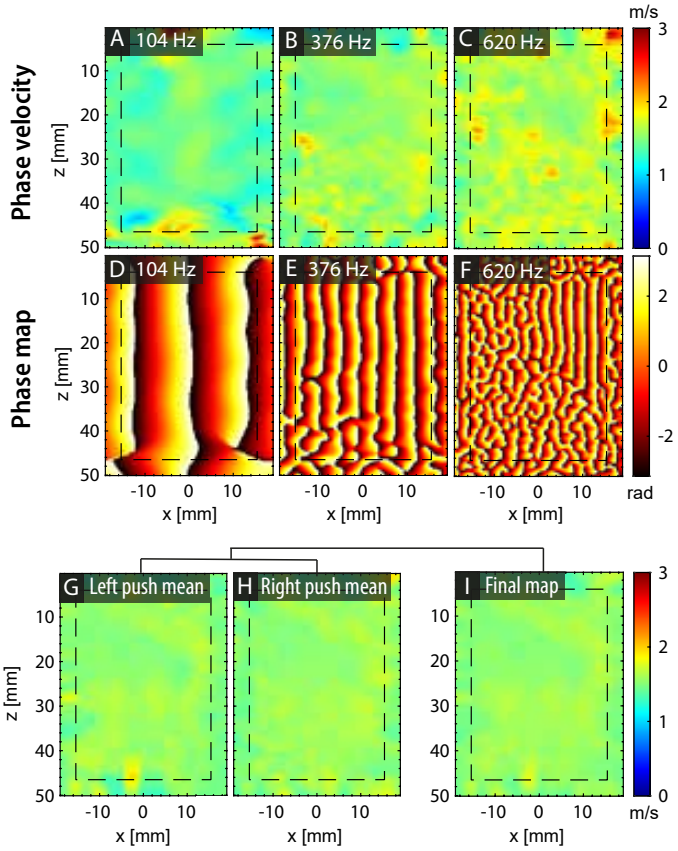


Fig. 2. Phase and phase velocity maps for the phantom I homogeneous are presented. Initially, both phase velocity (A-C) and phase (D-F) maps are plotted for varying frequencies between 100 and 600 Hz approximately for the left push beam case. Subsequently, the average velocity map for both left (G) and right (H) push and the final phase velocity map (I) resulting from averaging the latter two are plotted.

waves. The filtered spatial domain data $U_{\text{filt}}(x,z,\omega_0)$ are then obtained using an inverse two-dimensional Fourier transform (F_{2D}^{-1}).

To calculate the dominant wavenumber in the region of interest, the phase $\phi(x,z,\omega_0)$ of the filtered spectral data is first determined. Assuming a plane wave, the phase can be expressed as $\phi(x,z) \approx k_x x + k_z z + \phi_0$. The components k_x and k_z are computed by estimating the slope in both directions of the phase map, which is achieved using a second-order finite-difference approximation [14]. The wavevector components are obtained from this calculation, and the phase velocity map is derived as a function of frequency, using the dominant wavenumber such as, $c_{ph}(x,z,\omega_0) = 2\pi\omega_0/|\,\mathrm{Re}(\mathbf{k})|$

In the case of a homogeneous, elastic, isotropic, and incompressible soft tissue, the elasticity modulus E can be related to the phase velocity by $E = 3c_{ph}^2\rho_0$, where ρ_0 represents the density of the medium.

In this study, three distinct cases based on Acoustic Radiation Force (ARF) were analyzed. The first case considered a homogeneous medium, phantom I, while the other two included inclusions, one rigid and the other soft, phantom II and III respectively. Data acquisition was conducted using an L7-4 linear array transducer (Philips Healthcare, Andover, MA) and a Verasonics V1 system (Verasonics, Inc., Kirkland, WA). The push ultrasound frequency was set at 4.09 MHz, with detection pulses transmitted at 5.00 MHz. For imaging, plane wave compounding was employed using transmission angles of $-4°$, $0°$, and $+4°$, with a pulse repetition interval of 95 μs for each angle. Two IQ signals sets were obtained for each assumption, corresponding to ARF pushes to the left and right of the region of interest (ROI). The depth of the push beam was uniformly set to 17.6 mm across all cases.

III. Results

A. Homogeneous case

The initial analysis focuses on Phantom I, which consists of a homogeneous elastic medium. The spectral content of the shear wave motion is subsequently examined through a $k-\omega$

space analysis. For homogeneous media, the initial frequency is selected based on a 3 dB drop in the spectrum relative to the center frequency, while the final frequency is determined using a 12 dB drop criterion. The selected frequency range is $f = [104, 376, 620]$ Hz for both the left and right push conditions.

Figure 2(D-F) presents representative phase maps at the study frequencies, following the application of directional and wavenumber filtering. Figures 2(A-B) show the corresponding phase velocity maps for each frequency. To generate the final elastogram, two averaging steps are performed: first, phase velocity maps are averaged in the frequency domain for the left (Fig. 2G) and right push (Fig. 2H); second, the phase velocity maps obtained from each push are averaged, as shown in Fig. 2I. Accordingly, the final map is the mean of the six measurements, three of which pertain to frequency and two to push location. The time required for the generation of each map was 0.02 seconds, resulting in a total time of 0.12 seconds.

Directional and wavenumber filtering is a highly beneficial technique for the analysis of homogeneous media, as the selection of the filtering parameters is of paramount importance for the analysis of heterogeneous media. In the event of an inappropriate selection, the objects of the medium to be reconstructed may be deformed. The mean value of the rectangular area delineated in Fig. 2I is 1.58 m/s, with a minimum standard deviation of 0.05 m/s, resulting from averaging.

B. Heterogeneous case

The following section investigates the two heterogeneous cases, Phantom II and III, which differ based on the presence of a rigid inclusion in Phantom II and a soft inclusion in Phantom III. Both phantoms were subjected to an identical set of processing steps. Initially, wavenumber filtering was applied to the phase velocity of the inclusions in $k - \omega$ space. The phase velocity ranges for Phantom II and III were identified as $c_{\text{ph}} = [1, 2.5]$ m/s and $c_{\text{ph}} = [1.5, 3]$ m/s, respectively. These ranges encapsulate both the phase velocity values of the inclusions and the background medium. Additionally, directional filtering was performed on the left and right pushes to align with the shear wave's propagation direction within the region of interest (ROI).

For Phantom II, the frequency range was established as $f = [159, 620]$ Hz, while for Phantom III, the range extended to $f = [159, 756]$ Hz. Due to the lower signal-to-noise ratio in the velocity maps at individual frequencies, an averaging method was employed. This method averaged across three distinct frequency ranges, where each range comprises three phase velocity maps. Specifically, for Phantom II, these ranges were 159–321 Hz, 321–475 Hz, and 475–620 Hz, as shown in Fig. 3. For Phantom III, the corresponding ranges were 159–376 Hz, 376–566 Hz, and 566–756 Hz.

Reconstructing the push zone posed challenges in both phantoms. This difficulty stems from the fact that the phase pattern in the push zone deviates from a plane wave behavior,

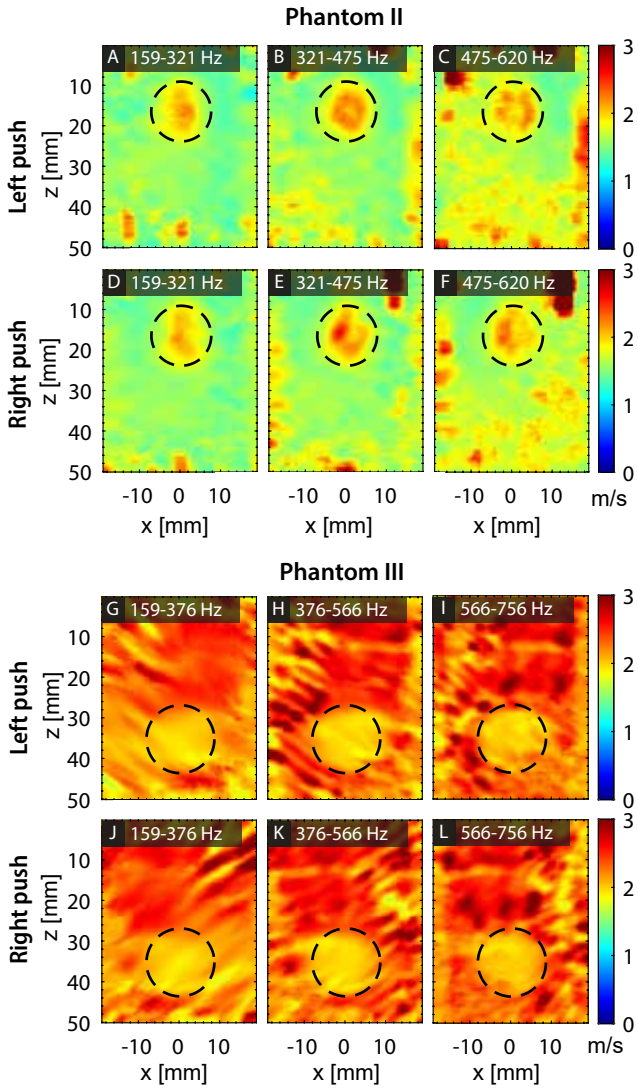


Fig. 3. Phase velocity maps for different frequencies for the phantom II (A-F) with a rigid inclusion and the phantom III with a soft inclusion (G-L). The maps presented for both phantoms represent the results obtained from both the left and right push of the inclusion. Furthermore, the mean map for distinct frequency ranges within the shear wave motion spectrum is presented.

as seen in Fig. 3C for a left-side push on the inclusion or Fig. 3F for a right-side push. At lower frequencies, while the noise levels were reduced, reconstruction accuracy declined. This decrease is attributed to the fact that the wavelength at these frequencies is significantly larger than the object being reconstructed. As the frequency increases, the inclusion's shape becomes more distinct (Fig. 3I and L). However, higher frequencies result in greater attenuation of shear waves, thereby reducing the quality of the reconstructed maps. To obtain an accurate reconstruction of the heterogeneous medium's inclusion, it is necessary to average over the full frequency bandwidth. This averaging corrects artifacts and improves the accuracy of the final phase velocity map.

The final maps for both phantoms represent the mean values for both frequency and push pulse location, illustrated in

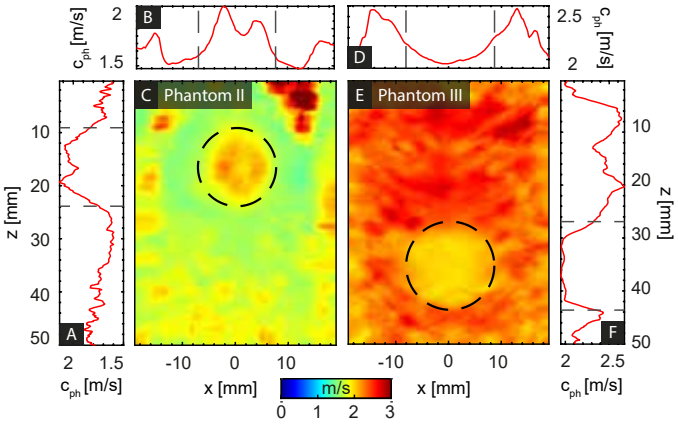


Fig. 4. The final phase velocity maps for Phantoms II (C) and III (E) are presented. Additionally, axial (A and F) and lateral (B-D) slices are plotted for each inclusion.

Fig. 4. Nine maps were constructed in the frequency domain, consisting of three maps for each analyzed range, as shown in Fig. 3. The final elastograms were obtained by averaging the reconstructed maps for both left and right pushes, resulting in each final map comprising 18 elastograms. Each elastogram was of dimension 324×247 pixels, with a reconstruction time of 0.014 seconds per map, and a total computation time of 0.253 seconds for the final map. Despite the proposed algorithm's lower robustness for individual frequency maps, its low computational complexity allows for real-time averaging of multiple elastograms, significantly reducing the standard deviation in the final map.

It is evident that the map reconstruction for the phantom II is suboptimal, Fig. 4C, as the detection of the inclusion zone and edges is not precise, resulting in an edge width of 4.05 mm with respect to the 14.78 mm diameter of the inclusion. One potential explanation for this discrepancy is the proximity of the push zone to the inclusion. In contrast, the reconstruction for the phantom III exhibits notable improvement, Fig. 4E, with enhanced edge detection and more precise localization, resulting in an edge width of 3.25 mm compared to the 16.72 mm diameter.

IV. Conclusions

In this study, we proposed a novel algorithm for wavenumber determination in elastography by integrating the angular spectrum method with a local phase gradient estimator. The results demonstrated the method's effectiveness in generating accurate phase velocity maps for both homogeneous and heterogeneous media, including phantoms with rigid and soft inclusions. The algorithm's low computational complexity makes it suitable for real-time applications, with the ability to significantly reduce noise and improve the precision of elastograms through directional and wavenumber filtering.

The phase velocity maps obtained for the homogeneous medium exhibited minimal standard deviation, confirming the robustness of the proposed methodology in this context. In the heterogeneous phantoms, while the inclusion boundaries were not perfectly reconstructed in the case of rigid inclusions, the algorithm provided improved performance for softer inclusions. Averaging across multiple frequency ranges and push conditions enhanced the accuracy of the final elastograms, ensuring detailed reconstructions despite signal attenuation at higher frequencies.

Overall, the proposed algorithm holds promise for improving the accuracy and computational efficiency of elastography in clinical and research settings. Future work may focus on refining the method for improved edge detection and further reducing artifacts, particularly in the case of heterogeneous media with complex structures.

References

[1] Muthupillai, R., Lomas, D., Rossman, P., Greenleaf, J., Manduca, A. & R. L. Ehman Magnetic Resonance Elastography by Direct Visualization of Propagating Acoustic Strain Waves. *Science*. **269**, 1854-1857 (1995)

[2] Ophir, J., Céspedes, I., Ponnekanti, H., Yazdi, Y. & Li, X. Elastography: A quantitative method for imaging the elasticity of biological tissues. *Ultrasonic Imaging*. **13**, 111-134 (1991)

[3] Bercoff, J., Tanter, M. & Fink, M. Supersonic shear imaging: a new technique for soft tissue elasticity mapping. *IEEE Transactions On Ultrasonics, Ferroelectrics, And Frequency Control*. **51**, 396-409 (2004)

[4] Myers, R., Elkashab, M., Ma, M., Crotty, P. & Pomier-Layrargues, G. Transient Elastography for the Noninvasive Assessment of Liver Fibrosis: A Multicentre Canadian Study. *Canadian Journal Of Gastroenterology And Hepatology*. **24**, 153986 (2010)

[5] Bercoff, J., Chaffai, S., Tanter, M., Sandrin, L., Catheline, S., Fink, M., Gennisson, J. & Meunier, M. In vivo breast tumor detection using transient elastography. *Ultrasound In Medicine & Biology*. **29**, 1387-1396 (2003)

[6] Chang, Y., Lo, W. & Liao, L. Surgeon-performed Ultrasound Elastography in the Evaluation of Thyroid Nodules. *Journal Of Medical Ultrasound*. **22**, 145-151 (2014)

[7] Chen, S., Urban, M., Pislaru, C., Kinnick, R., Zheng, Y., Yao, A. & Greenleaf, J. Shearwave dispersion ultrasound vibrometry (SDUV) for measuring tissue elasticity and viscosity. *IEEE Transactions On Ultrasonics, Ferroelectrics, And Frequency Control*. **56**, 55-62 (2009)

[8] Rouze, N., Wang, M., Palmeri, M. & Nightingale, K. Robust estimation of time-of-flight shear wave speed using a radon sum transformation. *IEEE Transactions On Ultrasonics, Ferroelectrics, And Frequency Control*. **57**, 2662-2670 (2010,12)

[9] Sugimoto, K., Moriyasu, F., Oshiro, H., Takeuchi, H., Yoshimasu, Y., Kasai, Y., Furuichi, Y. & Itoi, T. Viscoelasticity Measurement in Rat Livers Using Shear-Wave US Elastography. *Ultrasound In Medicine & Biology*. **44**, 2018-2024 (2018)

[10] Sandrin, L., Fourquet, B., Hasquenoph, J., Yon, S., Fournier, C., Mal, F., Christidis, C., Ziol, M., Poulet, B., Kazemi, F., Beaugrand, M. & Palau, R. Transient elastography: a new noninvasive method for assessment of hepatic fibrosis. *Ultrasound In Medicine & Biology*. **29**, 1705-1713 (2003)

[11] Kijanka, P. & Urban, M. Fast Local Phase Velocity-Based Imaging: Shear Wave Particle Velocity and Displacement Motion Study. *IEEE Transactions On Ultrasonics, Ferroelectrics, And Frequency Control*. **67**, 526-537 (2020,3), Conference Name: IEEE Transactions on Ultrasonics, Ferroelectrics, and Frequency Control

[12] Ormachea, J. & Parker, K. Reverberant shear wave phase gradients for elastography. *Physics In Medicine And Biology*. **66**, 175001 (2021,8)

[13] Pinton, G., Dahl, J. & Trahey, G. Rapid tracking of small displacements with ultrasound. *IEEE Transactions On Ultrasonics, Ferroelectrics, And Frequency Control*. **53**, 1103-1117 (2006,6)

[14] Fornberg, B. Generation of finite difference formulas on arbitrarily spaced grids. *Mathematics Of Computation*. **51**, 699-706 (1988)

[15] Manduca, A., Lake, D., Kruse, S. & Ehman, R. Spatio-temporal directional filtering for improved inversion of MR elastography images. *Medical Image Analysis*. **7**, 465-473 (2003,12)

[16] Song, P., Manduca, A., Zhao, H., Urban, M., Greenleaf, J. & Chen, S. Fast Shear Compounding Using Robust 2-D Shear Wave Speed Calculation and Multi-directional Filtering. *Ultrasound In Medicine & Biology*. **40**, 1343-1355 (2014,6)